# Simulator for Hydrologic Unstructured Domain (SHUD v1.0): Numerical modeling of watershed hydrology with the finite volume method

Lele Shu[1], Paul Ullrich[1], and Christopher Duffy[2]

[1]Department of Land, Air, and Water Resources, University of California, Davis, Davis, California 95616, USA
[2]Department of Civil and Environmental Engineering, Pennsylvania State University, University Park, Pennsylvania 16802, USA

**Correspondence:** Lele Shu (lele.shu@gmail.com)

**Abstract.** Hydrological modeling is an essential strategy for understanding and predicting natural flows, particularly where observations are lacking in either space or time, or where complex terrain leads to disconnect in the characteristic time and space scales of overland and groundwater flow. However, significant difficulties remain for the development efficient implementation of extensible modeling systems that operate robustly across complex regions. This paper introduces the Simulator for Hydrological Unstructured Domain (SHUD), an integrated, multi-process, multi-scale, multi- time-step model, in which hydrological processes are fully coupled using the Finite Volume Method. SHUD integrates overland flow, snow accumulation/melt, evapotranspiration, subsurface and groundwater flow, and river routing, which realistically captures the physical processes in a watershed. SHUD incorporates one-dimension unsaturated flow, two-dimension groundwater flow, and river channel network fully connected with hillslopes via overland flow and baseflow.

The paper introduces the design of SHUD, from the conceptual and mathematical description of hydrological processes in a watershed to computational structures. To demonstrate and validate the model performance, we employ three hydrological experiments: the V-Catchment experiment, Vauclin's experiment, and a model study of the Cache Creek Watershed in northern California, USA. Ongoing applications of SHUD model include hydrological analyses of the hillslope to regional scales ($1m$ to $10^6 km^2$), water resource and stormwater management, and interdisciplinary research with related fields in limnology, agriculture, geochemistry, geomorphology, water quality, and ecology, climatic and landuse change. The strength of SHUD is its' flexibility as a scientific or resource evaluation tool where modeling and simulation are required.

# 1 Introduction

The complexity of today's environmental issues, the multidiscilinary nature of scientific and resource management questions, and the diversity and incompleteness of available observational data, have all led to the need for models as a means of synthesis. When models are computationally efficient and physically consistent they become important tools for extrapolation across observations and systems that help us better understand the physical history of a given system or make decisions regarding the future, including socioeconomic, hydrological, or climatological. The data-sets produced through modeling can assist with decisions on infrastructural planning, water resource management, flood protection, contamination mitigation, and other relevant concerns. It is also important to note that the model complexity (resolution, scale, coupled states/fluxes) depends on the particular research or management purpose, the questions to be answered and the data availability.

Nonetheless, environmental managers policymakers, and stakeholders have a growing demand for high-resolution and detailed information about hydrological flows at fine temporal-spatial resolution across the watershed. This need reflects the growing importance detailed long-term predictions and projections for ecological systems and the environment, agricultural development, and food security under future climate change. Global climate modeling, typically performed with a general circulation model, also requires information on soil moisture and groundwater fluctuations, which are related to streamflow and reservoir management (Hrachowitz and Clark, 2017; Blöschl et al., 2019).

In hydrology lumped models (Hawkins et al., 1985; Fleming, 2010; Bergström, 1992) have proven to be fast and stable tools for estimating the outlet discharge in rivers, requiring simplified meteorological data and limited observed flow data. Lumped models disregard the spatial heterogeneity of terrestrial characteristics, while including the basic watershed features (e.g. contributing area, overall relief, average landuse, soil conditions, etc.). Their purpose is input-output analysis without internal structure (Moradkhani and Sorooshian, 2008) and their parameters may lack precise physical meaning which makes it challenging to interpret watershed characteristics or transfer parameters to other regions. On the other hand, distributed models (Beven, 2012; Lin et al., 2018; Gochis et al., 2015; Santhi et al., 2006; Liang et al., 1996; Vivoni et al., 2011; Refsgaard et al., 1998; Shen and Phanikumar, 2010) also have their limitations. One challenge for multi-process distributed models is addressing uncertainties in spatial parameters (soils, hydrogeology, land-surface processes, etc.) and limited predicitve skill for large, high-resolution catchments. Although the estimated model parameters (e.g. soil properties, surface characteristics, aquifer properties, iand atmospheric inputs have incomensurate resolutions. The latter is particularly important to watershed calibration leading to a major source of uncertainty (Beven, 2012; Blöschl et al., 2019). Nonetheless, at the continental and global scale progress has been made in higher resolution elevation data, refined soil surveys (Soil Survey Staff, 2015), satellite land cover (Homer and Fry, 2012) and much higher resolution atmospheric inputs which create new opportunities for the development of new hydrological models that leverage advances in data and in mathematical/computatiuonalg strategies.

The community has become more sophisticated about the choice of models (Beven, 2012) and the explicit purpose or application, ranging from the simplest lumped models (HEC-HMS (Fleming, 2010), HBV (Bergström, 1992)), to semi-distributed models (Beven, 1989; Beven and Germann, 1982; Beven and Kirkby, 1979), to complex distributed hydrological models (WRF-Hydro (Lin et al., 2018; Gochis et al., 2015),PRMS (Leavesley et al., 1983), SWAT (Santhi et al., 2006), VIC (Liang

et al., 1996), MIKE-SHE(Abbott and Refsgaard, 1996; Refsgaard et al., 1998), inHM (VanderKwaak, 1999), tRIBS (Vivoni et al., 2011, 2004, 2005) and PAWS (Shen and Phanikumar, 2010)), and even cutting-edge hydrological models based on machine-learning methods (Rasouli et al., 2012; Petty and Dhingra, 2018; Shen et al., 2018). In each case the choice model requires the assessment of factors related to prediction variables, performance, flexibility, and availability of data.

The Simulator for Hydrologic Unstructured Domain (SHUD) is a multi-process, multi-scale hydrological model where major hydrological processes are fully coupled using the Finite Volume Method (FVM). SHUD encapsulates the strategy for the synthesis of multi-state distributed hydrological models using the integral representation of the underlying physical process equations and state variables. As a heritage of Penn State Integrated Hydrologic Model (PIHM), the SHUD model is a continuation of 16 years of PIHM model development in hydrology and related fields since the release of its first PIHM version (Qu, 2004).

The conceptual structure of the *two-state integral-balance* model for soil moisture and groundwater dynamics is devised by (Duffy, 1996), in which the partial volumes occupied by unsaturated and saturated moisture storage were integrated directly upon local conservation equation. This two-state integral-balance structure simplified the hydrological dynamics while preserving the natural spatial and temporal scales contributing to runoff response. Brandes et al. (1998) use FEMWATER to realize the numeric calculation of inflow/outflow behavior within a hillslope-stream scheme. In 2004, Qu (2004) embedded the evapotranspiration and river network, and released Penn State Integrated Hydrologic Model (PIHM) v1.0, which is the most important milestone of the two-state integral-balance model. Since PIHM v1.0 (Qu, 2004), the PIHM is a generic hydrological model applicable to various watersheds or basins. After that, PIHM v2.0 (Kumar et al., 2009; Kumar and Duffy, 2009) enhance the land surface modeling. A GIS-tool, PIHMgis(Bhatt et al., 2014) and the Essential Terrestrial Variables Data Server (HydroTerre (Leonard and Duffy, 2013)) dramatically motivated the model deployment and applications with PIHM. Because of the sophisticated hydrological modeling and efficient spatial representative of PIHM, various model coupling project initialized. For example, Flux-PIHM coupled the NOAH Land Surface Model into PIHM to calculate more details in energy balance and evapotranspiration (Shi et al., 2015, 2014). Zhang et al. (2016) coupled the landscaping evolution with PIHM (LE-PIHM). Bao (Bao, 2016; Bao et al., 2017) coupled the reaction transport module with PIHM (RT-PIHM, RT-Flux-PIHM). Flux-PIHM-BGC (Shi et al., 2018) coupled the biogeochemistry into Flux-PIHM. The Multi-Module PIHM (MM-PIHM) project (https://github.com/PSUmodeling/MM-PIHM) planned to build a uniform repository for all coupled modules. Still, more PIHM coupling projects are ongoing, such as sediments, lakes, crops, etc.. In addition, a finite volume-based integrated hydrologic modeling (FIHM) was developed (Kumar et al., 2009), which used second-order accuracy and solved 2D unsteady overland flow and 3D subsurface flow. Figure 1 shows the family tree of PIHM and SHUD. Every revision/branch received cross-pollination from others. The PIHMgis and SHUDtoolbox are GIS, pre- and post-processing tools for PIHM and SHUD respectively.

Although PIHM and SHUD share the same fundamental conceptual two-state integral model, both the input/output are incompatible. Details of differences between them are summarised in the last section of this paper.
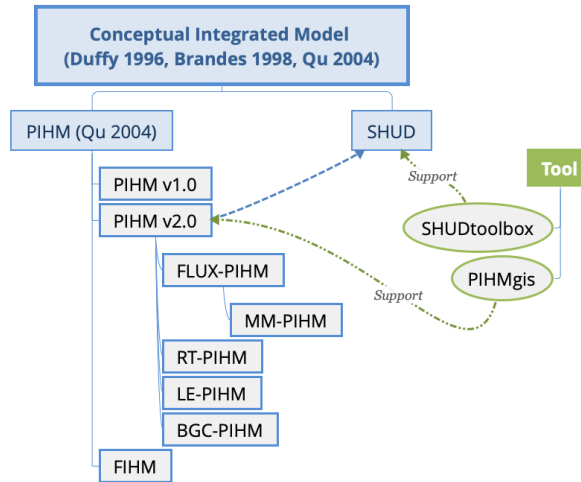
**Figure 1.** The family tree of PIHM and SHUD. PIHM and SHUD share the same fundamental conceptual model, but use different realization. The PIHMgis and SHUDtoolbox are GIS-tools for pre- and post-processing.

The SHUD's design is based on a concise representation of a watershed and river basin's hydrodynamics, which allows for interactions among major physical processes operating simultaneously, but with the flexibility to add or drop states-processes-constitutive relations depending on the objectives of the numerical experiment for research purpose.

The SHUD is a distributed hydrological model in which the domain is discretized using an unstructured triangular irregular network (e.g., Delaunay triangles) generated with constraints (geometric and parametric). A local prismatic control volume is formed by the vertical projection of the Delaunay triangles forming each layer of the model. Given a set of constraints (river network, watershed boundary, elevation, and hydraulic properties), an "optimized mesh" is generated. The "optimized mesh" allows the underlying coupled hydrological processes for each finite volume to be calculated numerical efficiently and stability (Farthing and Ogden, 2017; Vanderstraeten and Keunings, 1995; Shewchuk, 1996). We developed the R package SHUDtoolbox ( https://github.com/shud-system/SHUDtoolbox) helping users to generate the triangular domain. River volume cells are also prismatic, with trapezoidal or rectangular cross-section, and maintain the topological relation with the Delaunay triangles. The local control volumes encapsulate all equations to be solved and are herein referred to as the model kernel.

The objective of this paper is to introduce the design of SHUD, from the fundamental conceptual model of hydrology to governing hydrological equations in a watershed to computational structures describing hydrological processes. Section 2 describes the conceptual design and equations used in the model. In section 3, we employ three hydrological experiments to demonstrate the simulation and capacity of the model. The three applications presented here are (1) the V-Catchment experiment, (2) the Vauclin experiment (Vauclin et al., 1979), and (3) the Cache Creek Watershed (CCW), a headwater catchment in Northern California. Section 4 summarizes the differences between SHUD and PIHM, then proposes possible applications of the SHUD model.
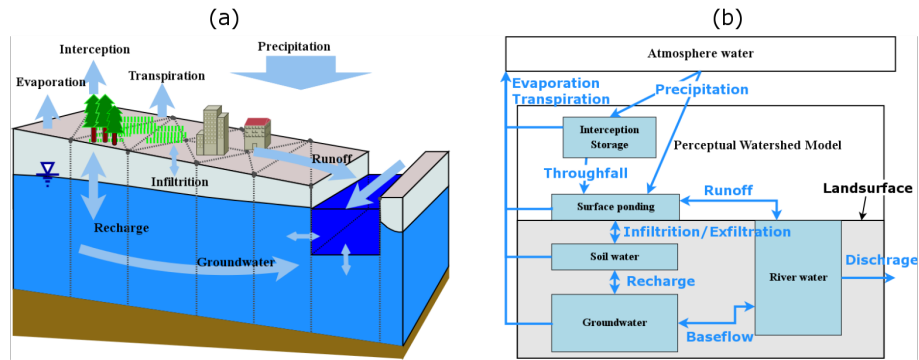
**Figure 2.** The conceptual schematic of hydrological processes in the SHUD model.

## 2 Model design

### 2.1 Conceptual description of hydrological system

We begin our introduction to the SHUD model with a conceptual description of water movement in a watershed (Fig. 2) describing processes that are incorporated in the model. Catchment hydrology is driven by atmospheric inputs including rainfall, snowfall and irrigation. The land surface hydrology first interacts with vegetation through plant-canopy interception and through-fall. When precipitation exceeds the interception capacity, through-fall or excess precipitation falls to the land surface. Snowfall accumulation and melting is an important land-surface process and a major source of soil moisture and recharge in many temperate or mountainous climate regions. SHUD captures the partitioning excess precipitation into surface runoff and infiltration into the soil.

Vertically, the aquifer is divided into two coupled layers based on its saturation status: the top unsaturated layer (or vadose layer) is constrained to 1-D vertical flow and saturated groundwater layer admits 2-D flow. These layers overlie an impermeable layer such as bedrock or an effective depth of circulation where deeper flows are small and unlikely to contribute to baseflow. The vertical fluxes within the unsaturated zone include infiltration and exfiltration. Deep percolation or recharge to a groundwater is fully coupled to soil moisture dynamics. SHUD accounts for conditions when the groundwater table reaches or exceeds the land surface, decreasing infiltration, allowing exfiltration as local ponding and runoff. The model also accounts for upward capillary flow from a shallow water table depending on soil moisture and vegetation conditions. Lateral (2-D) groundwater flow represents the basic mechanism for baseflow to streams or rivers.

Surface runoff or overland flow is generated by excess rainfall and ponding and is represented as a 2-D shallow water flow in SHUD. Surface runoff complements baseflow runoff as the dominant sources of streams or rivers. SHUD also allows reversing flows from the channel to the hillslope as surface inundation or channel losses to groundwater. This may occur when the river stage rises above bankfull storage during flooding events.

Evaporation generally represents the major water loss from the catchment with four components: evapotranspiration (ET) from interception storage, surface ponding, soil moisture and shallow groundwater. Transpiration occurs only when vegetation

5

is present and could draw from the saturated groundwater when the groundwater level is high enough. Direct evaporation occurs from interception, ponding water, and soil moisture.

Following the above description, several assumptions and simplifications are made in the SHUD model:

- In the default configuration, the watershed boundary is generally handled as a closed domain, in which precipitation/evapotranspiration are the major vertical fluxes and river flow is the major lateral flow into and out of the domain. Modifications to these conditions can be applied to realize additional flows such as pumping wells, irrigation, basin diversions,etc.. The model is able to specify boundary conditions based on the various research areas and purposes.

- The hydraulic gradient is vertical within the soil column and is controlled by gravity and capillary potential. This assumption is invalid for microscale soil water movement but useful when the model grid spacing ranges from meters to kilometers (Beven, 2012).

- The evaporative fluxes that occur due to ET from rivers is assumed to be small and can be approximated by the evapotranspiration from the riparian or hyporheic area of the model where shallow water table and high soil moisture conditions exist.

- The hydrological characteristics, including all physical parameters in soil, landuse, and terrain, are homogeneous within each cell. This is a common assumption in any distributed models, as the various models still need discretized domains instead of a continuous space.

- All geographic, topographic and hydraulic parameters do not change in time.

- Finally, SHUD uses a simplified representation of the geometry of the river networks due to the limitation of such data. This assumption is made because of the inherent challenges in measuring the geometry of the river cross-section everywhere along with the stream network.

## 2.2 Mathematical structure

The notation used in this section is summarized in list of symbols in the appendix.

Figure 3 depicts the geometric structure of the discrete cells in SHUD. The watershed domain is discretized using an irregular unstructured triangular network (Delaunay triangles) generated with imposed spatial constraints by Triangle (Shewchuk, 1996). The algorithm of triangulation is not limited to Delaunay, so any GIS software and advanced programming language (R, Matlab and Python) is capable to generate the triangular domain. A prismatic control volume is formed by the vertical extension of the Delaunay triangles to produce three layers: land surface layer, unsaturated zone, and groundwater layer. The modeler is responsible for defining the aquifer depth (from the land surface to the impervious bedrock) based on measurements or terrestrial characteristics. The thickness of the unsaturated zone ($D_{us}$) is determined by the difference between the land surface elevation ($z_{sf}$) and groundwater table ($z_{gw}$) above datum, i.e. $D_{us} = z_{sf} - z_{gw}$. When the groundwater table reaches the land surface ($z_{gw} > z_{sf}$), the thickness of unsaturated zone $\to 0$.
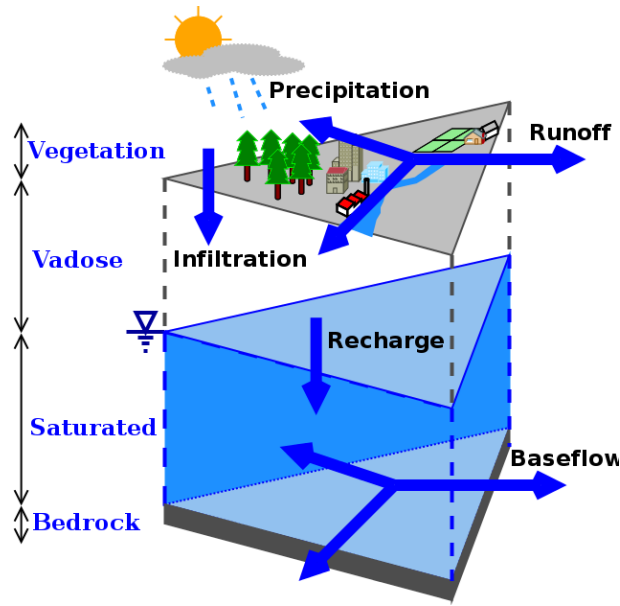
**Figure 3.** The three layers of the SHUD model and fluxes between layers.
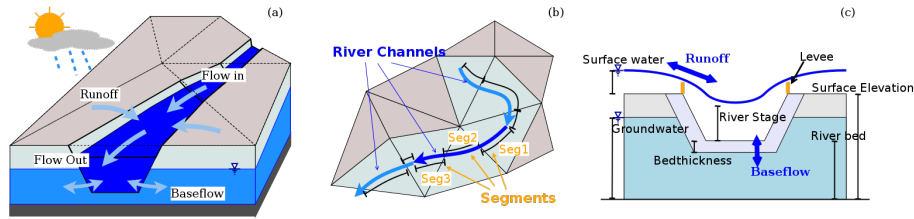


**Figure 4.** A depiction of the interaction between cells and the river network in the SHUD. (a) water balance in river channels, (b) topologic relationship between river channels and hillslope cells, and (c) water fluxes between river segments and hillslope cells.

Figure 4 depicts the exchange of water between the rivers and hillslope cells. Within each river channel, there are two longitudinal fluxes and two lateral fluxes: upstream ($Q_{up}$), downstream ($Q_{dn}$), overland ($Q_{sf}$) and groundwater ($Q_{sub}$).

The hydrological model uses the Method of Moments to reduce partial differential equations (PDE's) into ordinary differential equations (ODE's) and solves ODE system using a global implicit numerical solver. The state variables include water height on the land surface ($\boldsymbol{Y_{sf}}$), soil moisture storage ($\boldsymbol{Y_{us}}$), groundwater depth ($\boldsymbol{Y_{gw}}$), and river stage ($\boldsymbol{Y_{riv}}$). The initial value problem for these ODEs is formulated as

$$\frac{d\boldsymbol{Y}}{dt} = f(t, \boldsymbol{Y}), \qquad \boldsymbol{Y}(t_0) = \boldsymbol{Y_0},$$

7

**Table 1.** The governing equations in the SHUD model.

| Physical process | Method | Governing equation | Reference equation |
|---|---|---|---|
| Interception | Bucket model | $\frac{dS_{ic}}{dt} = P - E_{ic} - P_{tf}$ | 1 |
| Snow melt | Temperature Index Model | $\frac{dS_{sn}}{dt} = P - E_{sn} - q_{sm}$ | 9 |
| Overland flow | Diffusive Wave | $\frac{\partial h}{\partial t} + \frac{\partial (uh)}{\partial x} + \frac{\partial (vh)}{\partial y} = q$ | 11 |
| Unsaturated zone | Richards Equation | $C(\psi)\frac{\partial \psi}{\partial t} = \nabla - K(\psi) \cdot \nabla(\psi + Z)$ | 15 |
| Groundwater flow | Richards Equation | $C(\psi)\frac{\partial \psi}{\partial t} = \nabla - K(\psi) \cdot \nabla(\psi + Z)$ | 18 |
| River channel | St. Venant Equation (1D) | $\frac{\partial h}{\partial t} + \frac{\partial (uh)}{\partial x} = q$ | 25 |

where the discrete state vector is denoted by $\boldsymbol{Y}$,

$$\boldsymbol{Y} = \begin{pmatrix} \boldsymbol{Y_{sf}} \\ \boldsymbol{Y_{us}} \\ \boldsymbol{Y_{gw}} \\ \boldsymbol{Y_{riv}} \end{pmatrix},$$

$\boldsymbol{Y_0}$ are the initial conditions and $f(t, \boldsymbol{Y})$ denotes the equations governing the hydrological flow, which are described in this section.

The system of ODEs describing the hydrological processes are fully coupled and solved simultaneously at each time step ($\Delta t = t_n - t_{n-1}$) using CVODE, a stiff solver based on Newton-Krylov iteration (Hindmarsh et al., 2019). In brief, the CVODE solver calculates $\boldsymbol{Y}(t_n)$, given $\boldsymbol{Y}(t_{n-1})$ and $\frac{d\boldsymbol{Y}}{dt}|_{t_{n-1}}$. The technical description of the CVODE solver can be found in the literature (Hindmarsh et al., 2019, 2005; Cohen and Hindmarsh, 1996). The governing equations in SHUD are provided in table 1.

Figure 5 is the workflow within the SHUD model. The explicit model time step (MTS) $\Delta t = t_n - t_{n-1}$ is user-specified, typically varying from one minute to one hour. Within the MTS, all states are calculated and fluxes are determined by the relevant gradient law.

The change of fluxes of ET and interception within short period (such as one hour) are relative slow, so that full coupling of the ET with soil water is not necessary for this model. Instead, the interception, ET and snow calculations solved explicitly at MTS, while the calculation of $\boldsymbol{Y_{sf}}$, $\boldsymbol{Y_{us}}$, $\boldsymbol{Y_{gw}}$ and $\boldsymbol{Y_{riv}}$ use the implicit time step (ITS).

The CVODE solver determines the ITS automatically based on both the specified tolerances and the error function of $\boldsymbol{Y}$ and $d\boldsymbol{Y}$ in CVODE. The initial ITS is set equal to the explicit MTS. Within the ITS, $d\boldsymbol{Y}$s is calculated based on $\boldsymbol{Y}$ from the last MTS. If the CVODE solver converges with the current value of the ITS, it returns the updated $\boldsymbol{Y}$. Otherwise, a convergence failure occurs that forces an ITS reduction.

The introduction to the mathematical model underlying SHUD is now addressed in five components: vegetation and evapo-transpiration, land surface, unsaturated layer, saturated layer, and river channel.
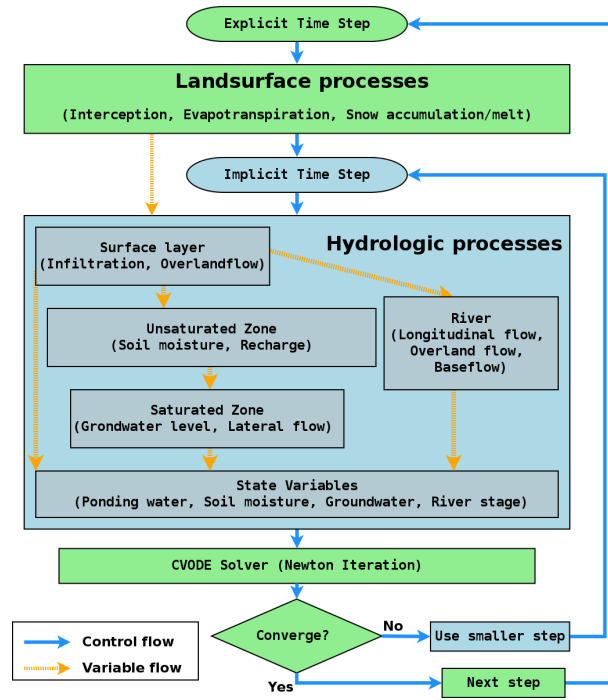
**Figure 5.** The flowchart demonstrates calculation of variables and time step control in the SHUD model. The hydrological processes are simulated in each finite volume cell, then the state variables ($Y$) are passed to the CVODE solver.

### 2.2.1 Vegetation and evapotranspiration

The interception is a direct water loss of precipitation when vegetation cover exists, and is treated as an simple storage *bucket* — namely, precipitation cannot reach the land surface until the interception storage capacity is satisfied. The capacity of this storage is the maximum interception volume, which is a function of the vegetation Leaf Area Index (LAI) and satisfies equation $S_{ic}^* = C_{ic}LAI$, where $LAI$ represents the coverage of vegetation canopy over the land area (area of leaves over area of land, $m^2/m^2$), and $C_{ic}$ is interception coefficient [$m$]. The default $C_{ic}$ is taken to be $0.2kg/m^2$ as suggested in Dickinson (1984).

The interception is equal to the deficit of interception – the difference between interception capacity ($S_{ic}^*$) and existing interception storage ($S_{ic}$). If precipitation is less than the deficit, interception is equal to the precipitation rate (see Fig. 6).

$$\frac{dS_{ic}}{dt} = q_{ic} - E_{ic} \tag{1}$$

$$q_{ic} = \begin{cases} \min[\frac{S_{ic}^*}{\Delta t}, P] & S_{ic} <= 0 \\ \min[\frac{(S_{ic}^* - S_{ic})}{\Delta t}, P] & 0 < S_{ic} < S_{ic}^* \\ 0 & S_{ic} >= S_{ic}^* \end{cases} \tag{2}$$
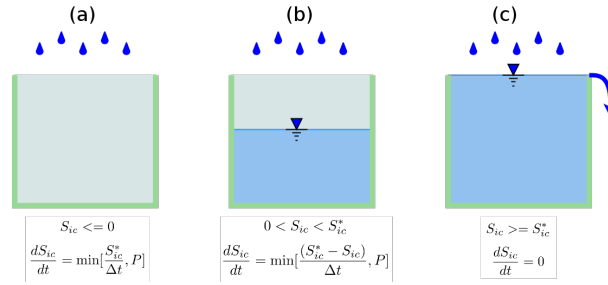
9

**Figure 6.** The three conditions for the interception calculation within the imaginary canopy *bucket*. The through-fall or excess precipitation after interception is the water gaining on the land surface.

Potential Evapotranspiration (PET) is the quantity of water that would evaporate and transpire from an ideal surface if extensive free water was available to meet the demand (Maidment, 1993; Kirkham, 2014). As such, PET is a practical and rapid estimation of water flux from land to atmosphere. The PET ($E_0$) is governed by Penman-Monteith equation(Penman, 1948):

$$E_0 = \frac{1}{\lambda} \frac{\Delta \left( R_n - G \right) + \rho_a c_p \frac{(e_s - e_a)}{r_a}}{\Delta + \gamma \left( 1 + \frac{r_s}{r_a} \right)}. \tag{3}$$

Here we do not elaborate on this equation, as it is common among different hydrological models (Allen, 1998; Maidment, 1993). At each ET step, the model calculates PET in terms of the prescribed forcing data. PET values are conditioned on the parameters from various land cover types, factored by varying albedo, LAI, and roughness length.

The total Actual Evapotranspiration (AET) consists of three parts: evaporation from interception($E_c$), transpiration from vegetation canopy ($E_t$) and direct evaporation of soil ($E_s$). The calculation of AET for these three components follows from the equations below:

$$
\begin{aligned}
E_c &= \max[S_{ic}/\Delta t, E_0], & (4) \\
E_s &= E_0 \beta_s (1 - \alpha_{imp})(1 - \alpha_{veg}), & (5) \\
E_t &= E_0 \beta_s (1 - \alpha_{imp}) \alpha_{veg}, & (6) \\
\beta_s &= \frac{\theta - \theta_r}{\theta_{fc} - \theta_r}. & (7)
\end{aligned}
$$

Here, $E_c$ is controlled by PET from interception storage. Both $E_s$ and $E_t$ are affected by soil water stress ($\beta_s$) and impervious area fraction ($\alpha_{imp}$). Impervious area is also considered a barrier of evapotranspiration in the model. $E_s$ is referred to as the demand water evaporation from soil, and emerges from two sources, namely the evaporation from ponding water ($E_{sp}$) and evaporation from soil moisture ($E_{sm}$), $E_s = E_{sp} + E_{sm}$. Ponded water has higher priority to evaporate and direct evaporation only uses the water in the surface when ponding water is able to meet the $E_s$ demand, i.e. $y_{sf}/\Delta t > E_s$. When ponding water

**10**

210  is insufficient to meet $E_s$, soil water balances the difference between demand and available water in the surface; when ponding water does not exist, direct evaporation extracts water from the soil profile ($E_{sm} = E_s, E_{sp} = 0$):

$$
\begin{cases}
E_{sp} = E_s, & E_{sm} = 0, & y_{sf} > E_s \times \Delta t, \\
E_{sp} = y_{sf}/dt, & E_{sm} = E_s - E_{sp}, & y_{sf} < E_s \times \Delta t, \\
E_{sp} = 0, & E_{sm} = E_s, & y_{sf} <= 0.
\end{cases}
\tag{8}
$$

Transpiration also has two potential sources: soil moisture and groundwater from the groundwater table and root depth for the land-use class. Once the groundwater table is higher than the root zone depth, vegetation uses groundwater, and soil
215  moisture stress for transpiration is equal to zero ($\beta_s = 0$).

Water balance associated with snow accumulation is quantified via

$$
\frac{dS_{sn}}{dt} = P_{sn} - q_{sn},
\tag{9}
$$

$$
q_{sn} = (T - T_0) \times m_f,
\tag{10}
$$

Snow melt rate is determined with snow melt factor ($m_f$), air temperature ($T$) and temperature threshold ($T_0$) at which snow
220  melt occurs. This formulation is often referred to as the degree-day method, in which the values of the snow melt factor and temperature threshold are empirical (Maidment, 1993; Beven, 2012). The water from snow melt is considered as a direct water contribution to the land surface.

### 2.2.2  Water on the land surface

Water balance on the land surface is given by:

225
$$
\frac{dy_{sf}}{dt} = P_n - E_{sp} - q_i - \sum_{j=1}^{3} \frac{Q_s^j}{A_c},
\tag{11}
$$

$$
P_n = P - S_{ic} + q_{sn},
\tag{12}
$$

$$
Q_s^j = \frac{L_j}{n} \overline{y_{sf}}^{\frac{5}{3}} s_0^{\frac{1}{2}},
\tag{13}
$$

The water balance of net precipitation ($P_n$), infiltration ($q_i$), evaporation from the ponding layer ($E_{sp}$) and horizontal overland flow ($Q_j$) determine the storage of water on the land surface. Net precipitation ($P_n$) is the total residual water after adjusting
230  for rainfall/snow interception and snowmelt. The overland flow $Q_s^j$ in direction $j$ is calculated with Manning's equation (13). Here $\overline{y_{sf}}$ is effective water height, determined by the gradient between two cells,

$$
\overline{y_{sf}} = \begin{cases}
y_{sf} & z_{sf} + y_{sf} >= z_{sf}^j + y_{sf}^j \\
y_{sf}^j & z_{sf} + y_{sf} < z_{sf}^j + y_{sf}^j
\end{cases}
\tag{14}
$$

Estimating infiltration utilizes Richards equation,

$$q_i = K_{ei}(\Theta)\left(1 + \frac{y_s}{D_{inf}}\right)$$

$$K_{ei}(\Theta) = \begin{cases} K_r(\Theta)k_x(1-\alpha_h) + \alpha_h k_m \Theta & y_s/\Delta t >= K_{max} \\ K_r(\Theta)k_x(1-\alpha_h) & y_s/\Delta t < K_{max} \end{cases}$$

$$K_r(\Theta) = \Theta^{\frac{1}{2}}\left(-1 + \left(1 - \Theta^{\frac{\beta}{\beta-1}}\right)^{\frac{\beta-1}{\beta}}\right)^2$$

$$K_{max} = k_x(1-\alpha_h) + \alpha_h k_m.$$

The infiltration rate is a function of soil saturation ratio ($\Theta$), soil properties ($k_x$, $k_m$ $\alpha$, $\beta$ and $\alpha_h$) and ponding water height (existing ponding water plus precipitation/irrigation). Infiltration occurs in the top soil layer ($D_{inf}$), and the infiltration rate is subjected to ponding water height and soil moisture. The default value of $D_{inf}$ is $10cm$, which can be changed in calibration files. The application rate $y_s/\Delta t$ combines ponding water, irrigation and precipitation together, and that determines the hydraulic gradient applied on the top soil layer. Finally, $K_{max}$ is the infiltration capacity determined by both soil matrix and macropore characteristics. When application rate is less than the maximum infiltration capacity, the infiltration is controlled by soil matrix flow; when application rate is larger than $K_{max}$, effective conductivity is a function of soil matrix and macropores(Chen and Wagenet, 1992). The infiltration equation takes the macropore effect into account, so the algorithm allows faster infiltration under heavy rainfall events and enables the soil to hold water for vegetation under dry condition.

### 2.2.3 Unsaturated zone

As discussed above, the horizontal flow in the vadose zone is neglected compared to the dominant vertical flow. There are three processes controlling the water in vadose zone: infiltration ($q_i$), ET in soil moisture ($E_{sm}$) and recharge to groundwater ($q_r$). The calculation of infiltration and ET is explained in the previous subsection. Recharge to groundwater is calculated with the equation 16. The soil moisture content to field capacity controls the recharge rate.

$$s_y \frac{dy_{us}}{dt} = q_i - q_r - E_{sm}, \tag{15}$$

$$q_r = K_{er}\left(\frac{\theta - \theta_r}{\theta_{fc} - \theta_r}\right) \tag{16}$$

$$K_{er} = \frac{D_{us} + y_{gw}}{D_{us}/k_x + y_{gw}/k_v}, \tag{17}$$

Because of the simplification of two-layer description of vertical aquifer profile, we use relationship between soil moisture and field capacity as the gradient to drive the recharge, instead of the hydraulic gradient. $K_{er}$ is the effective conductivity for recharge and is equal to the arithmetic mean of the conductivity of the unsaturated zone and saturated zone.

When the bottom of the vegetation root zone is below the groundwater table, then $E_{tg} > 0$ and vegetation extracts water from the saturated zone, otherwise $E_{tg} = 0$ meaning that transpiration uses soil moisture. When ponding water exists on the land surface, direct evaporation extracts water from ponding water first; when ponding water is depleted via evaporation, then the remainder of evaporation ($E_{sm}$) uses water from soil moisture based on the water stress.

### 2.2.4 Groundwater

The water balance of groundwater is controlled by the following equations:

$$s_y \frac{dy_{gw}}{dt} = q_r - E_{tg} - \sum_{j=1}^{3} \frac{Q_g^j}{A_c}, \tag{18}$$

$$Q_g^j = \overline{K} \cdot \frac{(y_{gw} + z_b) - (y_{gw}^j + z_b^j)}{d_j} \cdot (L_j \overline{y_{gw}}), \tag{19}$$

$$\overline{K} = (K_{eg} + K_{cg}^j) * 0.5. \tag{20}$$

The calculation of horizontal groundwater flow uses the Boussinesq equation. When the bottom of the root zone is lower than the groundwater table, then $E_t > 0$, otherwise, $E_t = 0$.

The horizontal groundwater flux $Q_g^j$ is determined by the Darcy equation and Dupuit-Forchheimer assumption. Above $z_b$ is the elevation of impervious bedrock, $z_b^j$ is the bedrock elevation of its $j$th neighbor cell and $d_j$ is distance between the centroids of two adjcent cells, so the gradient between the two cells is $\left[ (y_{gw} + z_b) - (y_{gw}^j + z_b^j) \right] d_j^{-1}$. The effective conductivity for the groundwater flow is the mean value of the effective horizontal conductivity over the two cells. The cross-sectional area along the groundwater flux is equal to $L_j \times \overline{y_{gw}}$.

In equation 20, the effective horizontal conductivity ($K_{eg}$) is a function of the groundwater table and characteristics of the macropores. The calculation of effective horizontal conductivity of each cell is given by

$$K_{eg} = \begin{cases} k_g, & z_m > z_{gw}, \\ \frac{z_{gw} - z_m}{y_{gw}} (k_m \alpha_v + (1 - \alpha_v) k_g) + k_g, & z_m < z_{gw}, \end{cases} \tag{21}$$

$$z_{gw} = y_{gw} + z_{cb}, \tag{22}$$

where $k_g$ and $k_m$ are the saturated hydraulic conductivity of soil matrix and macropores, $z_m$, $z_{gw}$ and $z_{cb}$ are elevations of macropore, groundwater table and bedrock, and $\alpha_v$ is the vertical areal macropore fraction [m$^2$/m$^2$].

The effective horizontal conductivity captures the effect of spatially varying conductivity on saturated flow when the groundwater level rises(Jiang et al., 2009; Bobo et al., 2012; Chen et al., 2018; Cheema, 2015; Taylor, 1960; Lin et al., 2007). Figure 7 reveals the effective horizontal conductivity changes along with different groundwater levels. When the groundwater table is below the level of the macropores, $K_{eg}$ is equal to saturated conductivity. When the groundwater level is above the macropore level, the effective conductivity increases with the groundwater level, taking into consideration the conductivity and area fraction of macropores in the soil profile. The maximum effective conductivity is achieved once the groundwater table level reaches the land surface.

### 2.2.5 Water in streams

The water balance in river channels is described by

$$\frac{dy_{riv}}{dt} = \frac{1}{A_r} \left( \sum_{j=1}^{j=N_c} Q_{sr}^j + \sum_{j=1}^{j=N_c} Q_{gr}^j + \sum_{j=1}^{j=N_u} Q_{up}^j + Q_{dn} \right). \tag{23}$$
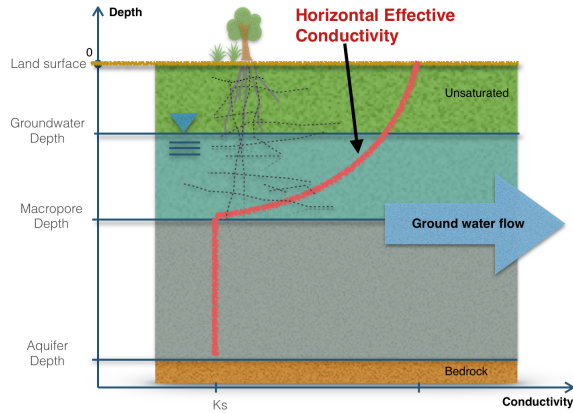
13

**Figure 7.** Effective conductivity for horizontal groundwater flow changes along the changing groundwater level. When the groundwater level is higher than macropore depth, groundwater flow increases due to the contribution of horizontal macropores.

The mass balance in each river channel consists of four parts: $Q_s^j$, the overland flow from cells (1 to $N_c$ cells) that intersect with the river channel; $Q_g^j$, the lateral groundwater flux from intersection with the $j$th cell; $Q_{up}^j$, the longitudinal flow from upstream channels; and $Q_{dn}$, the flux to the downstream channel. $N_u$ is the number of upstream channels; in the model, the number of upstream channels is nonnegative, but only one downstream channel is permitted. We assume river channels can converge to a single downstream channel. The convergence rule does not affect the topological relationship between river channels and cells.

The topological relationship between cells and river channels is shown in Fig. 4(b). As depicted, the river consists of a series of river reaches which intersect prismatic elements. A single reach is split as multiple river segments and each segment lies within a hillslope element. Surface and groundwater exchanges occur between each segment and the underlying cell. The sum of overland flow from multiple cells contributes to the net storage in a river reach.

The downstream channel flux $Q_{dn}$ is based on the one-dimensional diffusive wave equation that is simplified as Manning's equation for open channel:

$$Q_{dn} = \frac{A_{cs}}{\overline{n}} \left( \frac{A_{cs}}{\overline{P}} \right)^{\frac{2}{3}} \overline{s_0}^{\frac{1}{2}}, \tag{24}$$

where $A_{cs}$ is the cross-section area of the river reach, and $\overline{P}$ and $\overline{s_0}$ are average wet perimeter and average slope of a river reach and its downstream reach.

The upstream flux $Q_{up}$ is equal to the sum of $Q_{dn}$ from the multiple upstream reaches. The water balance equation in the river channel neglects evaporation and precipitation because the area of open water in the watershed is relatively small, and the area of open water is already included in pre-computation for the cells. Therefore, the channel routing represents the water exchange between the river and hillslope and takes the overland flow and baseflow into account.

The overland flow between river segment and associated hillslope cell ($Q_{sr}$) is calculated as follows:

$$Q_{sr} = L_s C_w b_s \sqrt{2g|b_s|}, \tag{25}$$

$$H_{riv} = y_{riv} + z_{rb}, \tag{26}$$

$$H_{csf} = y_{sf} + z_{cs}, \tag{27}$$

$$b_s = \begin{cases} H_{riv} - H_{csf}, & H_{riv} > z_{bank} \text{ and } H_{csf} > z_{bank}, \\ H_{riv} - z_{bank}, & H_{riv} > z_{bank} \text{ and } H_{csf} < z_{bank}, \\ H_{csf} - z_{bank}, & H_{riv} < z_{bank} \text{ and } H_{csf} > z_{bank}. \end{cases} \tag{28}$$

Here $z_{bank}$ is the elevation of riverbank or levee, implying that the relative height of the land surface or river stage controls the direction of water exchange between the land surface and river segment.

The groundwater exchange between river segment and hillslope cell is described by $Q_{gr}$, which is calculated as

$$Q_{gr} = L_s b_g K_{gr} \frac{H_{riv} - H_{cgw}}{d_{rb}}, \tag{29}$$

$$H_{cgw} = y_{gw} + z_{cb}, \tag{30}$$

$$b_g = \begin{cases} y_{riv}, & H_{cgw} < z_{rb}, \\ \frac{1}{2}(y_{riv} + H_{cgw} - z_{rb}), & H_{cgw} > z_{rb}, \end{cases} \tag{31}$$

$$K_{gr} = \frac{1}{2}(k_{rb} + K_{eg}). \tag{32}$$

## 3 Applications

In this section, we present the results of applying SHUD to three applications: first, we use the V-catchment experiment to validate the calculation of overland flow and river routing in an idealized catchment; second, we use Vauclin's experiment (Vauclin et al., 1979) to assess the calculation of infiltration, unsaturated flow in the vadose zone and horizontal saturated flow; finally, we apply the model to a hydrological simulation in the Cache Creek Watershed, a headwater catchment in Sacramento Watershed of Northern California.

### 3.1 V-Catchment

The V-Catchment (VC) experiment is a standard test case for numerical hydrological models to validate their performance for overland flow along a hillslope and in the presence of a river channel (Shen and Phanikumar, 2010). The VC domain consists of two inclined planes draining into a sloping channel (Fig. 8). Both hillslopes are $800 \times 1000m$ with Manning's roughness $n = 0.015$. The river channel between the hillslopes is 20 m wide and 1000 m in length with $n = 0.15$. The slope from the ridge to the river channel is 0.05 (in the $x$ direction), and the longitudinal slope (in the $y$ direction) is 0.02.

Rainfall in the VC begins at time zero at a constant rate of $18mm/hr$ and stops after 90 min, producing 27 mm of accumulated precipitation. Since evaporation and infiltration is not involved in this simulation, the total outflow from lateral boundaries and the river outlet must be the same as the total precipitation (following conservation of mass).
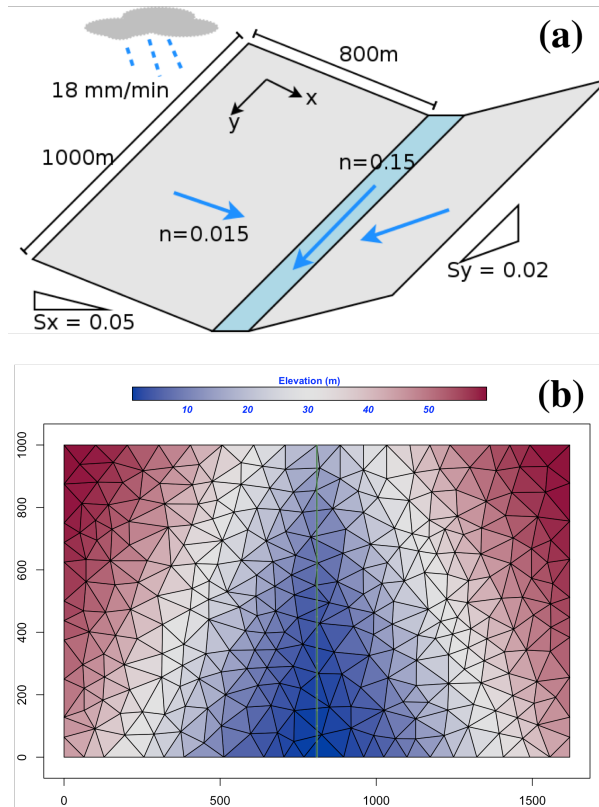
**Figure 8.** The tilted V-Catchment: (a) Basic structure of V-catchment, (b) the SHUD mesh used for the V-Catchment with elevation colored.

335      Figure 9 illustrates the discharge from the side-plane to the river channel and at the river outlet. The specific discharge (the volume discharge divided by the total area of the catchment) increases with precipitation until it reaches the maximum discharge rate, which is equal to the precipitation rate. Discharges along lateral boundaries and from the river outlet reach the maximum discharge rate, but at different times; namely, the discharge rate from the side-plane reaches the maximum value earlier than in the river outlet. The dots are discharge digitalized from Shen and Phanikumar (2010) with WebPlotDigitizer

340   (https://automeris.io/WebPlotDigitizer/). The results suggest SHUD can correctly capture the processes in overland flow and channel routing, although flow from the river outlet occurs earlier than the prediction in Shen and Phanikumar (2010). Both the fluxes from side-plane and outlet meet the maximum flow rate, that is the same magnitude of precipitation after a short period of rainfall. The flux rates start decreasing after precipitation stops. The accumulated volume of flux confirms the correct mass-balance of both fluxes.

345      To check numerical method, we verify the bias of mass-balance in the model and assess the differences among input, output and storage change in the system (equation 35). The bias in the model result is $\sim 0.2\%$.
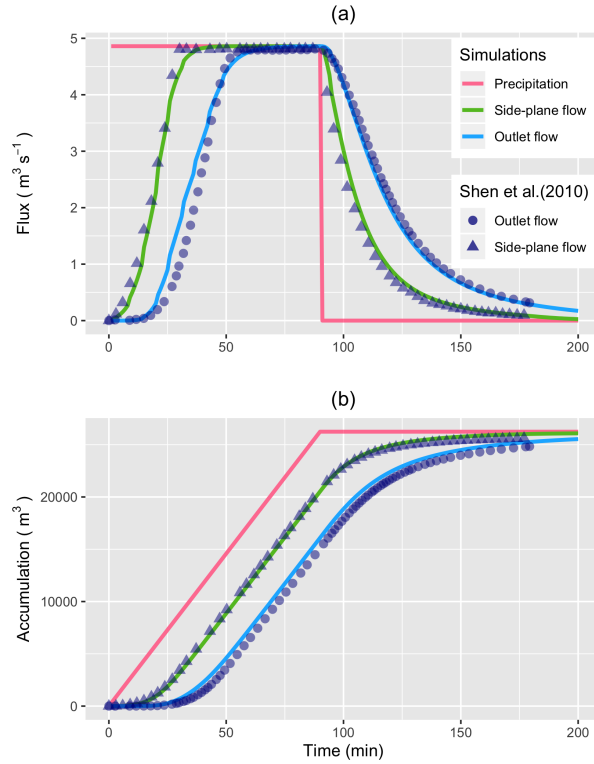
**Figure 9.** Comparison of overland flow and outflow at the outlet of the V-Catchment from the SHUD modeling versus Shen and Phanikumar (2010). (a) is volume fluxes while (b) is accumulated water volume.

$$\Delta S \quad = \quad P - Q - E \tag{33}$$

$$\hat{\Delta S} \quad = \quad \Delta S_{ic} + \Delta y_{sf} + \Delta y_{us} + \Delta y_{gw} + \Delta y_{riv} \tag{34}$$

$$Bias \quad = \quad \frac{|\hat{\Delta S} - \Delta S|}{\Delta S} \times 100\% \tag{35}$$

## 3.2 Vauclin's experiment

Vauclin's laboratory experiment (Vauclin et al., 1979) is designed to assess groundwater table change and soil moisture in the unsaturated layer under precipitation or irrigation. The experiment was conducted in a sandbox with dimension 3 m long $\times 2$ m deep $\times 0.05$ m wide (see Fig. 10). The box was filled with uniform sand particles with measured hydraulic parameters: the saturated hydraulic conductivity was 35 cm/hr and porosity was $0.33$ m$^3$/m$^3$. The left and bottom of the sandbox were impervious layers, and the top and the right side were open. The hydraulic head was set to be constant at 0.65m on the right boundary. Constant irrigation (1.48 cm/hr) was applied over the first 50 cm of the top-left of the sandbox while the rest of the top was covered to avoid water loss via evaporation.
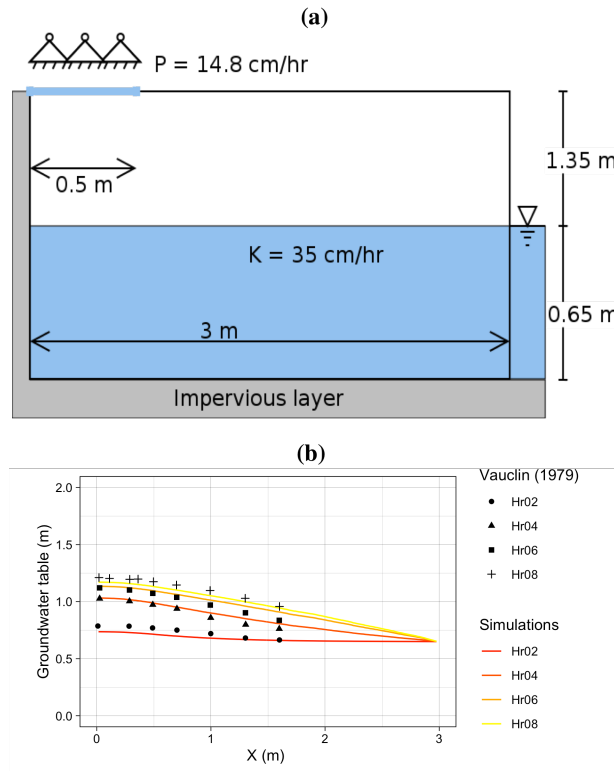
**Figure 10.** A schematic of (a) Vauclin's experiment and (b) a comparison of Vauclin's measurements versus simulated groundwater table change with SHUD.

The experiment's initial condition is an equilibrium water table with a uniform hydraulic head. Irrigation was initiated at $t = 0$. The groundwater table was then measured at 2, 4, 6, and 8 hours at several locations along the length of the box. (Vauclin et al., 1979) also use 2-D (vertical and horizontal) numeric model to simulate the soil moisture and groundwater table. The maximum bias between measurement and simulation was $0.52m$, according to the digitalized value of Vauclin et al., 1979, Fig. 10.

Besides the parameters specified in (Vauclin et al., 1979), additional information is needed by the SHUD, including the $\alpha$ and $\beta$ in the van Genutchen equation and residual water content ($\theta_r$). Therefore, we use a calibration tool to estimate the representative values of these parameters. The use of calibration in this simulation is reasonable because the model – inevitably – simplifies the real hydraulic processes. The calibration thus nudges the parameters to *representative* values that approach or fit the *true* natural processes. The calibrated values are $\theta_r = 0.001m^3/m^3$, $\alpha = 0.3$ and $\beta = 5.2$. The simulated results in our modeling and literatures (Vauclin et al., 1979; Shen and Phanikumar, 2010) show a modest error between the simulations and measurements.

This error is likely due to (1) the need for more detailed aquifer layer description of soil layers or (2) the validity of the vertical and horizontal flow assumptions in the SHUD model.
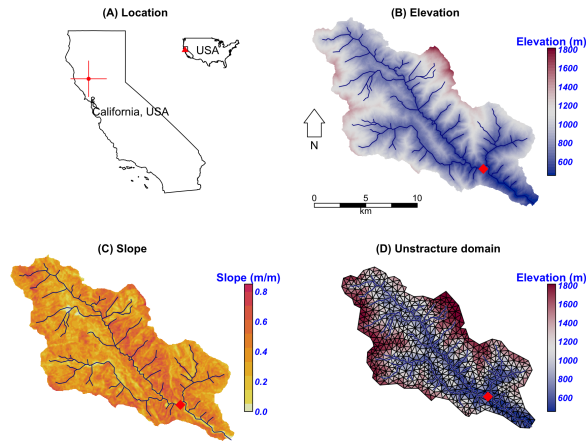
**Figure 11.** The location, terrestrial and hydrological description of the Cache Creek in California. The red diamond in the map is the USGS gage station (11451100) used for calibration and validation.

SHUD simulated the groundwater table at all four measurement points (see Fig. 10(b)). The maximum bias between simulation and Vauclin's observations is $5.5cm$, with $R^2 = 0.99$, that is comparable to the bias $5.2cm$ of numerical simulation in (Vauclin et al., 1979). By adding more layer structure, the bias in simulation decreases to $3cm$. Certainly, the simplifications employed by SHUD for the unsaturated and saturated zone benefits the computation efficiency while limiting the applicability where fine-scale soil profile information is required.

The simulations, compared against Vauclin's experiment, generally validate the algorithm for infiltration, recharge, and lateral groundwater flow. More reliable vertical flow within unsaturated layer requires multiple layers, which is planned in next version of SHUD.

### 3.3 Cache Creek Watershed

The Cache Creek Watershed (CCW) is a headwater catchment with area $196.4km^2$ in the Sacramento Watershed in Northern California (Figures 11 (a), (b) and (c)). The elevation ranges from $450m$ to $1800m$, with a $0.38m/m$ average slope which is very steep, and hence a particularly difficult watershed for hydrologic models to simulate.

Based on NLDAS-2 from 2000 to 2017 the mean temperature and precipitation was $12.8°C$ and $\sim 817mm$, respectively, in this catchment. Precipitation is unevenly distributed through the year, with winter and spring precipitation being the vast majority of the contribution to the annual total (Fig. 12).

Table 2 lists the geospatial and forcing data supporting the hydrological modeling in CCW. The DEM is 30-meter resolution raster data from National Elevation Dataset(NED)(U.S. Geological Survey, 2016). Forcing data, including precipitation, temperature, relative humidity, wind speed, and net radiation, is from NLDAS-2 ((Xia et al., 2012) https://ldas.gsfc.nasa.gov/nldas/v2/forcing). Our simulation in CCW covers the period from 2000 to 2007. Because of the Mediterranean climate in this
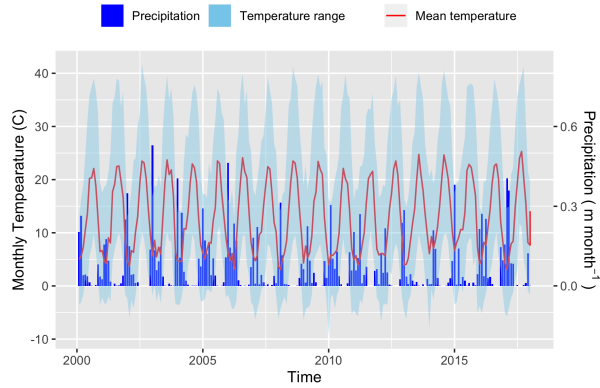
**19**

**Figure 12.** The monthly precipitation and temperature in Cache Creek based on NLDAS-2 data from 2000 to 2018. The blue ribbon is monthly precipitation in $m/month$; the red line is monthly mean temperature while blue shadow is the minimum and maximum temperature.

| Data | Data Source | Type | Resolution |
|------|-------------|------|------------|
| Hydrology | NHD plus(McKay et al., 2012) | Vector | - |
| Elevation | NED(U.S. Geological Survey, 2016) | Raster | 30m |
| Soil | gSSURGO(Soil Survey Staff, 2015) | Vector | - |
| Land-use | NLCD2006(Homer and Fry, 2012) | Raster | 30m |
| Climate | NLDAS-2 FORA(Xia et al., 2012) | Raster | 1/8 deg |

**Table 2.** The basic data sources used to build the model domain of the Cache Creek Watershed.

region, the simulation starts in summer to ensure adequate time before the October start to the water year. In our experiment, the first year (2000-06-01 to 2001-06-30) is the spin-up period, the following two years (2001-07-01 to 2003-06-30 ) are the calibration period, and the period from 2003-07-01 to 2007-07-01 is for validation.

The unstructured domain of the CCW (Fig. 11 (d)) is built with SHUDtoolbox. The number of triangular cells is 1147, with a mean area of $0.17km^2$. The total length of the river network is $126.5km$ and consists of 103 river reaches and in which the highest order of stream is 4. With a calibrated parameter set, the SHUD model tooks 5 hours to simulate 18 years (2000-2017) in the CCW, with a non-parallel configuration (OpenMP is disabled on Mac Pro 2013 Xeon 2.7GHz, 32GB RAM).

Figure 13 reveals the comparison of simulated discharge against the observed discharge at the gage station of USGS 11451100 (https://waterdata.usgs.gov/ca/nwis/uv/?site_no=11451100). The calibration procedure exploits the Covariance Matrix Adaptation – Evolution Strategy (CMA-ES) to calibrate automatically (Hansen, 2016). The calibration program assigns 72 children in each generation and keeps the best child as the seed for next-generation, with limited perturbations. The perturbation for the next generation is generated from the covariance matrix of the previous generation. After 23 generations, the calibration tool identifies a locally optimal parameter set.
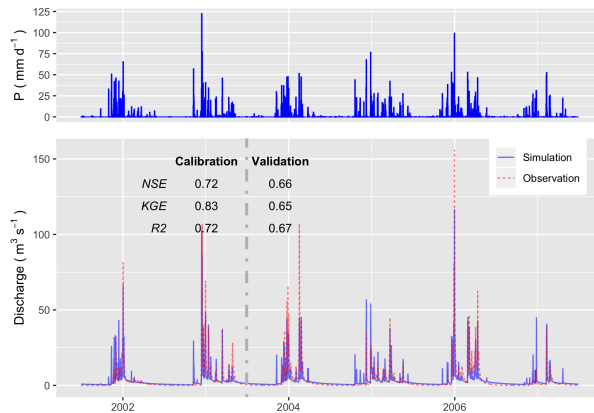
**Figure 13.** The hydrograph in Cache Creek (simulation versus observation) in the calibration (2001-07-01 to 2003-06-30) and validation periods (2003-07-01 to 2007-06-30).

In the calibration period, Nash-Sutcliffe efficiency (NSE Nash and Sutcliffe (1970)), Kling-Gupta Efficiency (KGE, Gupta
405  et al. (2009)) and $R^2$ is 0.72, 0.83 and 0.72 respectively (Fig. 13. The goodness-of-fit in the validation period is less than calibration period (as expected), with NSE = 0.66, KGE = 0.67 and $R^2 = 0.65$. Although the SHUD model captures the flood peaks after rainfall events, the magnitude of high flow in the hydrograph is less than the gage data. There are two potential causes of this bias: (1) underestimated precipitation intensity from NLDAS-2 data, or (2) over-fitting in the calibration, as the NSE tends to capture the mean value of the observational data rather than the extremes.

410  Figure 14 represents the monthly water balance in CCW, in which the PET is three times the annual precipitation, but the actual evapotranspiration (AET) is only 27% of the precipitation. This result emerges because the summer is the peak of PET, while winter is the peak of precipitation and water availability. The AET is subjected to PET and water availability, so the maximum of AET occurs in early summer. The runoff ratio is about 73%.

We use the groundwater distribution (Fig. 15) to demonstrate the spatial distribution of hydrological metrics calculated from
415  the SHUD model. Figure 15 illustrates the annual mean groundwater table in the validation period. Because the model fixes a $30m$ aquifer, the results represent the groundwater within this 30-meter aquifer only. The groundwater table and elevation along the green line on the upper map are extracted and plotted in the bottom figure. The gray ribbon is the 30-meter aquifer, and the blue line is the location where groundwater storage is larger than zero. The green polygons with the right axis are the groundwater storage along the cross-section. The groundwater levels tend to follow the terrain, with groundwater accumulated
420  in the valley, or along relatively flat flood plains. In the CCW, groundwater does not stay on steep slopes suggesting the high conductivity of upland slopes.

## 4  Summary

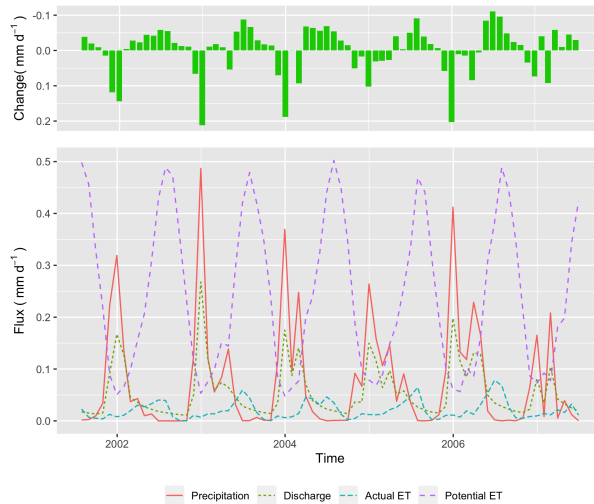A summary of the formulation and results.

**Figure 14.** The monthly water balance trends in Cache Creek Watershed from 2001-07-01 to 2007-06-30. Top: net change of water storage; Bottom: fluxes of precipitation, actual evapotranspiration, potential evapotranspiration and discharge at the outlet.

– SHUD is a physically-based process spatially distributed catchment model. The model applies national geospatial data resources to simulate surface and subsurface flows in gaged or ungaged cathcments. SHUD represents the spatial heterogeneity that influences the hydrology of the region based the national soils data and surficial geology. Several other groups have used PIHM, a SHUD ancester to couple processes for biochemistry, reaction transport, landscape, geomorphology, limnology and other related research areas.

– SHUD is a fully-coupled hydrological model, where the conservative hydrological fluxes are calculated within the same time step. The state variables are the height of ponding water on the land surface, soil moisture, groundwater level, and river stage, while fluxes are infiltration, overland flow, groundwater recharge, lateral groundwater flow, river discharge, and exchange between river and hillslope cells.

– The global ODE system solved in SHUD solves with a state-of- the-art parallel ODE solver, known as CVODE (Hindmarsh et al., 2005) developed at the Lawrence Livermore National Laboratory.

– SHUD permits adaptable temporal and spatial resolution. The spatial resolution of the model varies from centimeters to kilometers based on modeling requirements computing resources. The internal time step of the iteration is adjustable and adaptive; it can export the status of a catchment at time-intervals from minutes to days. The flexible spatial and temporal resolution of the model is valuable for community model coupling.

– SHUD can estimate either a long-term hydrological yield or a single-event flood.

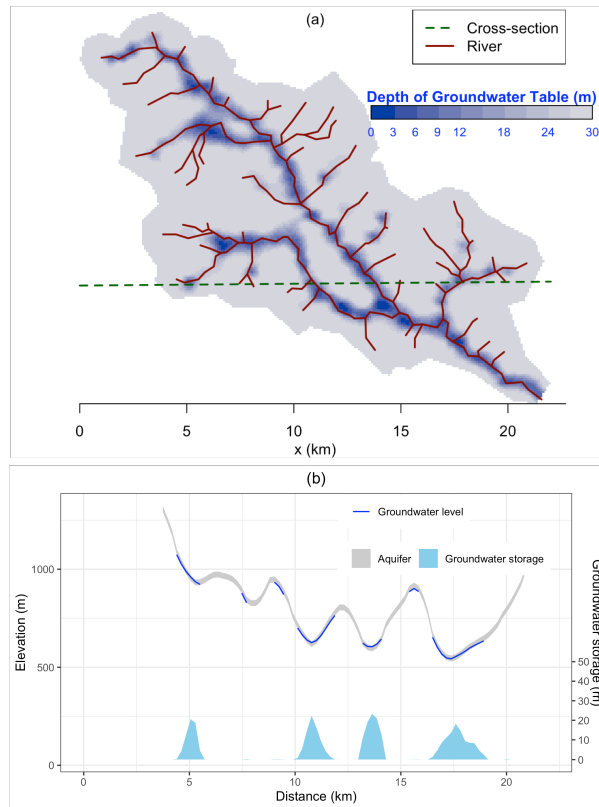– SHUD is an open-source model — available on github.

**Figure 15.** groundwater table (top) and the storage of groundwater (bottom) in $30m$ depth aquifer. The groundwater table and elevation along the green line on the top map are extracted and plot in the bottom figure. The gray ribbon is the 30-meter aquifer, and the blue line is the groundwater table, only at the location where groundwater storage is larger than zero. The green polygons with the right axis are the groundwater storage along the cross-section line.

## 4.1 Differences from PIHM

As a descendant of PIHM, SHUD inherits the fundamental idea of conceptual structure and solving hydrological variables in CVODE. The code has been completely rewritten in a new programming language, with a new discretization and corresponding improvements to the underlying algorithms, adapting new mathematical schemes and a new user-friendly input/output data format. Although SHUD is forked from PIHM's track, SHUD still inherits the use of CVODE for solving the ODE system but modernizes and extends PIHM's technical and scientific capabilities. The major differences are the following:

1. SHUD is written in C++, an object-oriented programming language with functionality to avoid risky memory leaks from C. Every function in the code has been rewritten, so the functions, algorithm or data structure between SHUD and PIHM are incompatible.

2. SHUD implements a re-design of the calculation of water exchange between hillslope and river. The PIHM defines the river channel as adjacent to bank cells – namely, the river channel shares the edges with bank cells. This design leads to sink problems in cells that share one node with a starting river channel, and fatherly slow down the performance of the simulation.

3. Although the mathematical equations underlying SHUD are generally the same as PIHM, the numerical formulation of processes, the coupling strategy and input/output has been greatly enhanced.

4. SHUD adds mass-balance control within the calculation of each layer of cells and river channels, important for accurate and efficient long-term and micro-scale hydrologic modeling.

5. The internal data structure and external input/output formats have been redesigned for efficiency and user-friendly formats supporting ASCII and Binary. Binary format is particularly important for efficiently writing and post-processing very large models.

We now briefly summarize the technical model improvements and technical capabilities of the model, compared to PIHM. This elaboration of the relevant technical features aims to assist future developers and advanced users with model coupling. Compared with PIHM, SHUD ...

– supports the latest implicit Sundial/CVODE solver to version 5.0.0 (the most recent version at the time of writing) and above,

– supports OpenMP parallel computation,

– redesigns the program with object-oriented programming (C++),

– supports human-readable input/output files and filenames,

– exposes unified functions to handle the time-series data, including forcing, leaf area index, roughness length, boundary conditions and melt factor,

– exports model initial condition at specific intervals that can be used for warm starts of continued simulation,

– automatically checks the range of physical parameters and forcing data,

– adds a debug mode that monitors potential errors in parameters and memory operations.

– includes a range a R codes for pre- and post-processing data, visualization, and data analysis (that will be discussed in another paper).

# 5 Conclusions

The Simulator for Hydrologic Unstructured Domain (SHUD) is a multi-process, multi-scale and multi-temporal hydrological model that integrates major hydrological processes and solves the physical hydrological equations with the Finite Volume Method. The governing hydrological equations are solved within an unstructured mesh domain — triangular cells. The variables in the surface, vadose layer, groundwater and river routing are fully coupled together with a very fine time-step. The SHUD uses one-dimensional unsaturated flow and two-dimensional groundwater flow. River channels connect with hillslope via overland flow and baseflow. The model, while using distributed terrestrial characteristics (from climate, land use, soil and geology) and preserving their heterogeneity, supports efficient performance through parallel computation.

SHUD is a robust integrated modeling system that has the potential for providing scientists with new insights into their domains of interest and will benefit the development of coupling approaches and architectures that can incorporate scientific principles. The SHUD modeling system can be used for applications in (1)hydrological studies from hillslope scale to regional scale; area of the model domain ranges from $1\ m$ to $10^6 km^2$ (2) water resource and stormwater management, (3) coupling research with related fields, such as limnology, agriculture, geochemistry, geomorphology, water quality, and ecology, (4) climate change, and (5) land-use change. In summary, SHUD is a valuable scientific tool for any modeling task associating with hydrological responses.

*Code and data availability.* The source code of SHUD model is kept updating at https://github.com/SHUD-System/SHUD. The code and data used for this page is archived at ZENODO:

SHUD model: 10.5281/zenodo.3561293.

User manual: 10.5281/zenodo.3561293.

V-catchment: 10.5281/zenodo.3566022

Vauclin(1979) experiment: 10.5281/zenodo.3566020

Cache Creek Watershed: 10.5281/zenodo.3566036

**Appendix: Nomenclature**

**Evapotranspiration Calculation**

$\Delta$      Slope vapour pressure curve $[kPaC^{-1}]$

$\gamma$      Psychrometric constant $[kPaC^{-1}]$

$\lambda$      Latent heat of vaporization $[MJkg^{-1}]$

$\rho_a$      Density of Air $[kgm^{-3}]$

505    $c_p$        Specific heat at constant pressure $[MJkg^{-1}C^{-1}]$

$e_a$        Actual vapour pressure $[kPa]$

$e_s$        Saturation vapour pressure $[kPa]$

$G$        Soil heat flux density $[MJm^{-2}s^{-1}]$

$r_a$        Aerodynamic resistance $[sm^{-1}]$

510    $r_s$        Surface resistance of vegetation $[sm^{-1}]$

$R_n$        Net radiation at the crop surface $[MJm^{-2}s^{-1}]$

**Hydrological metrics**

$\alpha$        van Genutchten soil parameter $[m^{-1}]$

$\alpha_h$        Horizontal macropore areal fraction $[m^2m^{-2}]$

515    $\alpha_{imp}$        Impervious area fraction $[m^2m^{-2}]$

$\alpha_{veg}$        Vegetation fraction $[m^2m^{-2}]$

$\alpha_v$        Vertical macropore areal fraction $[m^2m^{-2}]$

$\bar{K}$        Average conductivity $[ms^{-1}]$

$\bar{y}$        Effective height of overland flow between two adjacent cells $[m]$

520    $\beta$        van Genutchten soil parameter $[-]$

$\beta_s$        Soil moisture stress to evapotranspiration $[-]$

$\Delta t$        Time interval between consequential time steps $[m]$

$\overline{y_{gw}}$        Effective water height for groundwater flow calculation $[m]$

$\overline{y_{sf}}$        Effective water height for overland flow calculation $[m]$

525    $\psi$        Soil matrix potential head $[m]$

$\Theta$        Relative saturation ratio $[-]$

$\theta$        Soil moisture content $[m^3m^{-3}]$

$\theta_r$        Residual soil moisture content $[m^3m^{-3}]$

$\theta_s$      Porosity of soil $[m^3 m^{-3}]$

530    $\theta_{fc}$      The soil moisture content of field capacity $[m^3 m^{-3}]$

$A_c$      Area of a cell $[m^2]$

$A_r$      Area of river open water $[m^2]$

$b_g$      Effective height of groundwater flow between the river segment and hillslope cell $[m]$

$b_s$      Effective height of overland flow between the river segment and hillslope cell $[m]$

535    $C_{ic}$      Coefficient of interception $[m]$

$C_w$      Coefficient of discharge $[m]$

$d_j$      Distance between centroids of the current cell and neighbor $j$ $[m]$

$d_{rb}$      Thickness of river bed; for calculation of baseflow to rivers $[m]$

$D_{us}$      The deficit of soil column; thickness of vadose layer $[m]$

540    $E_0$      Potential evapotranspiration $[ms^{-1}]$

$E_c$      Evaporation from interception $[ms^{-1}]$

$E_{sm}$      Evaporation from the soil matrix $[ms^{-1}]$

$E_{sp}$      Evaporation from ponding water on land surface $[ms^{-1}]$

$E_s$      Evaporation from soil $[ms^{-1}]$

545    $E_{tg}$      Transpiration from saturated layer $[ms^{-1}]$

$E_t$      Transpiration $[ms^{-1}]$

$H_{cgw}$    Hydraulic head of water in cell groundwater $[m]$

$H_{csf}$    Hydraulic head of water on land surface $[m]$

$H_{riv}$    Hydraulic head in a river channel $[m]$

550    $k_m$      Saturated conductivity of soil macropore $[ms^{-1}]$

$K_r(\Theta)$    Relative conductivity, which is a function of saturation ratio $[-]$

$k_x$      Saturated conductivity of the top soil $[ms^{-1}]$

$K_{eg}$     Effective horizontal conductivity $[ms^{-1}]$

$K_{ei}(\Theta)$     Effective infiltration conductivity $[ms^{-1}]$

555    $K_{er}$     Effective recharge conductivity $[ms^{-1}]$

$k_g$     Saturated horizontal conductivity $[ms^{-1}]$

$k_{rb}$     Saturated conductivity of the river bed $[-]$

$k_v$     Saturated vertical conductivity of saturated layer $[ms^{-1}]$

$L_j$     Length of edge $j$ of a cell $[m]$

560    $L_s$     Length of river segment that overlay with a cell $[m]$

$LAI$     Leaf Area Index $[m^2 m^{-2}]$

$m_f$     Snow melting factor $[ms^{-1}C^{-1}]$

$n$     Manning's roughness $[sm^{-1/3}]$

$N_c$     Number of cells overlaying a river reach $[-]$

565    $N_u$     Number of upstream reaches flowing to a river reach $[-]$

$P$     Atmospheric precipitation or irrigation $[ms^{-1}]$

$P_n$     Net precipitation $[ms^{-1}]$

$P_{sn}$     Snowfall $[ms^{-1}]$

$Q_{dn}$     Volume flux to the downstream river channel $[m^3 s^{-1}]$

570    $Q_{gr}$     Volume flux between river and cells via groundwater flow $[m^3 s^{-1}]$

$Q_g$     Groundwater flow between two cells $[m^3 s^{-1}]$

$q_i$     Infiltration rate, positive is downward $[ms^{-1}]$

$q_r$     Recharge rate, positive is downward $[ms^{-1}]$

$q_{sn}$     Snow melting rate $[ms^{-1}]$

575    $Q_{sr}$     Volume flux between river and hillslope cells via overland flow $[m^3 s^{-1}]$

$Q_s$     The overland flow between two cells $[m^3 s^{-1}]$

$Q_{up}$      Volume flux from upstream river reaches $[m^3 s^{-1}]$

$s_y$      Specific yield $[mm^{-1}]$

$s_0$      The slope of land surface $[mm^{-1}]$

580    $S_{ic}$      Water storage of interception layer (canopy) $[m]$

$S_{ic}^*$      Maximum interception capacity $[m]$

$S_{sn}$      Snow storage $[m]$

$T$      Air temperature $[C]$

$T_0$      Temperature threshold for snowmelt to occur $[C]$

585    $y_{gw}$      Groundwater head (above impervious bedrock) of a cell $[m]$

$y_{riv}$      River stage in a river channel $[m]$

$y_{sf}$      Surface water storage in a cell $[m]$

$y_{us}$      Unsaturated storage equivalence of a cell $[m]$

$z_{bank}$      Elevation of the riverbank from the datum $[m]$

590    $z_b$      Elevation of impervious bedrock from the datum $[m]$

$z_{gw}$      Elevation of groundwater table from the datum $[m]$

$z_m$      Elevation of macropore from the datum $[m]$

$z_{sf}$      Elevation of land surface from the datum $[m]$

**Variables used in CVODE**

595    $\mathbf{Y_0}$      The initial conditions to start the simulation. $[m]$

$\mathbf{Y_{gw}}$      Vector of cell groundwater head (above impervious bedrock) $[m]$

$\mathbf{Y_{riv}}$      Vector of river stage in all river channels $[m]$

$\mathbf{Y_{sf}}$      Vector of surface water storage of all cells $[m]$

$\mathbf{Y_{us}}$      Vector of unsaturated storage equivalence of all cells $[m]$

600    $\mathbf{Y}$      Vector of conserved state variables in CVODE $[m]$

$t$        Time $[s]$

$t_n$        Current time $[s]$

$t_{n-1}$        Previous time $[s]$

*Competing interests.* Paul Ullrich is a member of the editorial board of the journal

# References

Abbott, M. B. and Refsgaard, J. C., eds.: Distributed Hydrological Modelling, vol. 22 of *Water Science and Technology Library*, Springer Netherlands, Dordrecht, https://doi.org/10.1007/978-94-009-0257-2, 1996.

Allen, R. G.: Crop evapotranspiration - Guidelines for computing crop water requirements - FAO Irrigation and drainage paper 56, FAO, 1998.

Bao, C.: Understanding Hydrological And Geochemical Controls On Solute Concentrations At Large Scale, Ph.D. thesis, Pennsylvania State University, 2016.

Bao, C., Li, L., Shi, Y., and Duffy, C.: Understanding watershed hydrogeochemistry: 1. Development of RT-Flux-PIHM, Water Resources Research, 53, 2328–2345, https://doi.org/10.1002/2016WR018934, 2017.

Bergström, S.: The HBV model - its structure and applications, Tech. rep., 1992.

Beven, K.: Changing ideas in hydrology - The case of physically-based models, Journal of Hydrology, 105, 157–172, https://doi.org/10.1016/0022-1694(90)90161-P, 1989.

Beven, K.: Rainfall-Runoff Modelling, John Wiley & Sons, Ltd, Chichester, UK, https://doi.org/10.1002/9781119951001, 2012.

Beven, K. and Germann, P. F.: Macropores and water flows in soils, Wat. Resour. Res., 18, 1311–1325, https://doi.org/10.1029/WR018i005p01311, 1982.

Beven, K. J. and Kirkby, M. J.: A physically based, variable contributing area model of basin hydrology, Hydrological Sciences Bulletin, 24, 43–69, https://doi.org/10.1080/02626667909491834, 1979.

Bhatt, G., Kumar, M., and Duffy, C. J.: A tightly coupled GIS and distributed hydrologic modeling framework, Environmental Modelling and Software, 62, 70–84, https://doi.org/10.1016/j.envsoft.2014.08.003, 2014.

Blöschl, G., Bierkens, M. F., and et. al.: Twenty-three unsolved problems in hydrology (UPH) – a community perspective, Hydrological Sciences Journal, 64, 1141–1158, https://doi.org/10.1080/02626667.2019.1620507, 2019.

Bobo, A. M., Khoury, N., Li, H., and Boufadel, M. C.: Groundwater flow in a tidally influenced gravel beach in prince william sound, alaska, Journal of Hydrologic Engineering, 17, 478–494, https://doi.org/10.1061/(ASCE)HE.1943-5584.0000454, 2012.

Brandes, D., Duffy, C. J., and Cusumano, J. P.: Stability and damping in a dynamical model of hillslope hydrology, Water Resources Research, 34, 3303–3313, https://doi.org/10.1029/98WR02532, http://doi.wiley.com/10.1029/98WR02532, 1998.

Cheema, T.: Depth dependent hydraulic conductivity in fractured sedimentary rocks-a geomechanical approach, Arabian Journal of Geosciences, 8, 6267–6278, https://doi.org/10.1007/s12517-014-1603-8, 2015.

Chen, C. and Wagenet, R.: Simulation of water and chemicals in macropore soils Part 1. Representation of the equivalent macropore influence and its effect on soilwater flow, Journal of Hydrology, 130, 105–126, https://doi.org/10.1016/0022-1694(92)90106-6, 1992.

Chen, Y. F., Ling, X. M., Liu, M. M., Hu, R., and Yang, Z.: Statistical distribution of hydraulic conductivity of rocks in deep-incised valleys, Southwest China, Journal of Hydrology, 566, 216–226, https://doi.org/10.1016/j.jhydrol.2018.09.016, 2018.

Cohen, S. D. and Hindmarsh, A. C.: CVODE, a stiff/nonstiff ODE solver in C, Computers in physics, 10, 138–143, https://doi.org/10.1063/1.4822377, 1996.

Dickinson, R. E.: Modeling Evapotranspiration for Three-Dimensional Global Climate Models, Climate Processes and Climate Sensitivity, 29, 58–72, https://doi.org/10.1029/GM029p0058, 1984.

Duffy, C. J.: A two-state integral-balance model for soil moisture and groundwater dynamics in complex terrain, Water Resources Research, 32, 2421–2434, https://doi.org/10.1029/96WR01049, 1996.

650     Farthing, M. W. and Ogden, F. L.: Numerical Solution of Richards' Equation: A Review of Advances and Challenges, Soil Science Society of America Journal, 81, 1257, https://doi.org/10.2136/sssaj2017.02.0058, 2017.

Fleming, M. J.: Hydrologic Modeling System HEC-HMS Quick Start Guide, U.S Army Corps of Engineers, 2010.

Gochis, D., Yu, W., and Yates, D.: The NCAR WRF-Hydro Technical Description and User's Guide, version 3.0. NCAR Technical Document, Tech. Rep. May, NCAR, 2015.

655     Gupta, H. V., Kling, H., Yilmaz, K. K., and Martinez, G. F.: Decomposition of the mean squared error and NSE performance criteria: Implications for improving hydrological modelling, Journal of Hydrology, 377, 80–91, https://doi.org/10.1016/j.jhydrol.2009.08.003, 2009.

Hansen, N.: The CMA Evolution Strategy: A Comparing Review, in: Towards a New Evolutionary Computation, pp. 75–102, Springer-Verlag, Berlin/Heidelberg, https://doi.org/10.1007/11007937_4, 2016.

Hawkins, R. H., Hjelmfelt, A. T., and Zevenbergen, A. W.: Runoff probability, storm depth, and curve numbers, Journal of Irrigation and
660     Drainage Engineering, 111, 330–340, https://doi.org/10.1061/(ASCE)0733-9437(1985)111:4(330), 1985.

Hindmarsh, A. C., Brown, P. N., Grant, K. E., Lee, S. L., Serban, R., Shumaker, D. E., and Woodward, C. S.: {SUNDIALS}: Suite of nonlinear and differential/algebraic equation solvers, ACM Transactions on Mathematical Software (TOMS), 31, 363–396, 2005.

Hindmarsh, A. C., Serban, R., and Reynolds, D. R.: User documentation for CVODE v5.0.0, Tech. rep., Center for Applied Scientific Computing Lawrence Livermore National Laboratory, 2019.

665     Homer, C. and Fry, J.: The National Land Cover Database, US Geological Survey Fact Sheet, 2012.

Hrachowitz, M. and Clark, M. P.: HESS Opinions: The complementary merits of competing modelling philosophies in hydrology, Hydrology and Earth System Sciences, https://doi.org/10.5194/hess-21-3953-2017, 2017.

Jiang, X. W., Wan, L., Wang, X. S., Ge, S., and Liu, J.: Effect of exponential decay in hydraulic conductivity with depth on regional groundwater flow, Geophysical Research Letters, 36, 3–6, https://doi.org/10.1029/2009GL041251, 2009.

670     Kirkham, M.: Potential Evapotranspiration, in: Principles of Soil and Plant Water Relations, chap. Chapter 28, pp. 501–514, Elsevier, https://doi.org/10.1016/B978-0-12-420022-7.00028-8, 2014.

Kumar, M. and Duffy, C. J.: Detecting hydroclimatic change using spatio-temporal analysis of time series in Colorado River Basin, Journal of Hydrology, 374, 1–15, https://doi.org/10.1016/j.jhydrol.2009.03.039, 2009.

Kumar, M., Duffy, C. J., and Salvage, K. M.: A Second-Order Accurate, Finite Volume-Based, Integrated Hydrologic Modeling (FIHM)
675     Framework for Simulation of Surface and Subsurface Flow, Vadose Zone Journal, 8, 873–890, https://doi.org/10.2136/vzj2009.0014, 2009.

Leavesley, G. H., Lichty, R. W., Troutman, B. M., and Saindon, L. G.: Precipitation-runoff modeling system; user's manual, Tech. rep., USGS, Denver, Colorado, https://doi.org/10.3133/wri834238, 1983.

Leonard, L. and Duffy, C. J.: Essential Terrestrial Variable data workflows for distributed water resources modeling, Environmental Modelling
680     & Software, 50, 85–96, https://doi.org/10.1016/j.envsoft.2013.09.003, 2013.

Liang, X., Lettenmaier, D. P., and Wood, E. F.: One-dimensional statistical dynamic representation of subgrid spatial variability of precipitation in the two-layer variable infiltration capacity model, Journal of Geophysical Research, 101, 21 403, https://doi.org/10.1029/96JD01448, 1996.

Lin, L., Jia, H., and Xu, Y.: Fracture network characteristics of a deep borehole in the Table Mountain Group (TMG), South Africa, Hydro-
685     geology Journal, 15, 1419–1432, https://doi.org/10.1007/s10040-007-0184-y, 2007.

Lin, P., Yang, Z. L., Gochis, D. J., Yu, W., Maidment, D. R., Somos-Valenzuela, M. A., and David, C. H.: Implementation of a vector-based river network routing scheme in the community WRF-Hydro modeling framework for flood discharge simulation, Environmental Modelling and Software, 107, 1–11, https://doi.org/10.1016/j.envsoft.2018.05.018, 2018.

Maidment, D. R.: Handbook of hydrology, vol. 9780070, McGraw-Hill New York, 1993.

690 McKay, L., Bondelid, T., Dewald, T., Johnston, J., Moore, R., and Rea, A.: NHDPlus version 2: user guide, Tech. rep., US Environmental Protection Agency, 2012.

Moradkhani, H. and Sorooshian, S.: General Review of Rainfall-Runoff Modeling: Model Calibration, Data Assimilation, and Uncertainty Analysis, in: Hydrological Modelling and the Water Cycle, pp. 1–24, Springer Berlin Heidelberg, Berlin, Heidelberg, https://doi.org/10.1007/978-3-540-77843-1_1, 2008.

695 Nash, J. E. and Sutcliffe, J. V.: River Flow Forecasting Through Conceptual Models Part I-a Discussion of Principles*, Journal of Hydrology, 10, 282–290, https://doi.org/10.1016/0022-1694(70)90255-6, 1970.

Penman, H. L.: Natural evaporation from open water, hare soil and grass, Proceedings of the Royal Society of London. Series A, Mathematical and physical sciences, https://doi.org/10.1098/rspa.1948.0037, 1948.

Petty, T. R. and Dhingra, P.: Streamflow Hydrology Estimate Using Machine Learning (SHEM), Journal of the American Water Resources
700 Association, https://doi.org/10.1111/1752-1688.12555, 2018.

Qu, Y.: An integrated hydrologic model for multi-process simulation using semi-discrete finite volume approach, Ph.D. thesis, Pennsylvanis State University, 2004.

Rasouli, K., Hsieh, W. W., and Cannon, A. J.: Daily streamflow forecasting by machine learning methods with weather and climate inputs, Journal of Hydrology, 414-415, 284–293, https://doi.org/10.1016/J.JHYDROL.2011.10.039, 2012.

705 Refsgaard, J. C., Sørensen, H. R., Mucha, I., Rodak, D., Hlavaty, Z., Bansky, L., Klucovska, J., Topolska, J., Takac, J., Kosc, V., Enggrob, H. G., Engesgaard, P., Jensen, J. K., Fiselier, J., Griffioen, J., and Hansen, S.: An integrated model for the Danubian Lowland - methodology and applications, Water Resources Management, https://doi.org/10.1023/A:1008088901770, 1998.

Santhi, C., Srinivasan, R., Arnold, J. G., and Williams, J. R.: A modeling approach to evaluate the impacts of water quality management plans implemented in a watershed in Texas, Environmental Modelling and Software, 21, 1141–1157,
710 https://doi.org/10.1016/j.envsoft.2005.05.013, 2006.

Shen, C. and Phanikumar, M. S.: A process-based, distributed hydrologic model based on a large-scale method for surface-subsurface coupling, Advances in Water Resources, 33, 1524–1541, https://doi.org/10.1016/j.advwatres.2010.09.002, 2010.

Shen, C., Laloy, E., Elshorbagy, A., Albert, A., Bales, J., Chang, F. J., Ganguly, S., Hsu, K. L., Kifer, D., Fang, Z., Fang, K., Li, D., Li, X., and Tsai, W. P.: HESS Opinions: Incubating deep-learning-powered hydrologic science advances as a community, Hydrology and Earth
715 System Sciences, https://doi.org/10.5194/hess-22-5639-2018, 2018.

Shewchuk, J. R.: Triangle: Engineering a 2D quality mesh generator and Delaunay triangulator, in: Applied Computational Geometry Towards Geometric Engineering, edited by Lin, M. C. and Manocha, D., pp. 203–222, Springer Berlin Heidelberg, Berlin, Heidelberg, 1996.

Shi, Y., Davis, K. J., Zhang, F., Duffy, C. J., and Yu, X.: Parameter estimation of a physically based land surface hydrologic model using the
720 ensemble Kalman filter: A synthetic experiment, Water Resources Research, 50, 706–724, https://doi.org/10.1002/2013WR014070, 2014.

Shi, Y., Baldwin, D. C., Davis, K. J., Yu, X., Duffy, C. J., and Lin, H.: Simulating high-resolution soil moisture patterns in the Shale Hills watershed using a land surface hydrologic model, Hydrological Processes, 29, 4624–4637, https://doi.org/10.1002/hyp.10593, 2015.

Shi, Y., Eissenstat, D. M., He, Y., and Davis, K. J.: Using a spatially-distributed hydrologic biogeochemistry model with a nitrogen transport module to study the spatial variation of carbon processes in a Critical Zone Observatory, Ecological Modelling, https://doi.org/10.1016/j.ecolmodel.2018.04.007, 2018.

Soil Survey Staff: Gridded Soil Survey Geographic (gSSURGO) Database for the Conterminous United States, Tech. rep., United States Department of Agriculture, 2015.

Taylor, G. S.: Drainable porosity evaluation from outflow measurements and its use in drawdown equations, https://doi.org/10.1097/00010694-196012000-00004, 1960.

U.S. Geological Survey: USGS National Elevation Dataset (NED) 1 arc-second Downloadable Data Collection from The National Map 3D Elevation Program (3DEP) - National Geospatial Data Asset (NGDA), Tech. rep., U.S. Geological Survey, 2016.

VanderKwaak, J. E.: Numerical simulation of flow and chemical transport in integrated surface-subsurface hydrologic systems, Ph.D. thesis, University of Waterloo, 1999.

Vanderstraeten, D. and Keunings, R.: Optimized partitioning of unstructured finite element meshes, International Journal for Numerical Methods in Engineering, 38, 433–450, https://doi.org/10.1002/nme.1620380306, 1995.

Vauclin, M., Khanji, D., and Vachaud, G.: Experimental and numerical study of a transient, two-dimensional unsaturated-saturated water table recharge problem, Water Resources Research, 15, 1089–1101, https://doi.org/10.1029/WR015i005p01089, 1979.

Vivoni, E. R., Ivanov, V. Y., Bras, R. L., and Entekhabi, D.: Generation of Triangulated Irregular Networks Based on Hydrological Similarity, Journal of Hydrologic Engineering, 9, 288–302, https://doi.org/10.1061/(asce)1084-0699(2004)9:4(288), 2004.

Vivoni, E. R., Ivanov, V. Y., Bras, R. L., and Entekhabi, D.: On the effects of triangulated terrain resolution on distributed hydrologic model response, Hydrological Processes, 19, 2101–2122, https://doi.org/10.1002/hyp.5671, 2005.

Vivoni, E. R., Mascaro, G., Mniszewski, S., Fasel, P., Springer, E. P., Ivanov, V. Y., and Bras, R. L.: Real-world hydrologic assessment of a fully-distributed hydrological model in a parallel computing environment, Journal of Hydrology, 409, 483–496, https://doi.org/10.1016/j.jhydrol.2011.08.053, 2011.

Xia, Y., Mitchell, K., Ek, M., Sheffield, J., Cosgrove, B., Wood, E., Luo, L., Alonge, C., Wei, H., Meng, J., Livneh, B., Lettenmaier, D., Koren, V., Duan, Q., Mo, K., Fan, Y., and Mocko, D.: Continental-scale water and energy flux analysis and validation for the North American Land Data Assimilation System project phase 2 (NLDAS-2): 1. Intercomparison and application of model products, Journal of Geophysical Research Atmospheres, https://doi.org/10.1029/2011JD016048, 2012.

Zhang, Y., Slingerland, R., and Duffy, C.: Fully-coupled hydrologic processes for modeling landscape evolution, Environmental Modelling & Software, 82, 89–107, https://doi.org/10.1016/j.envsoft.2016.04.014, 2016.